MOLECULAR AND CELLULAR BIOLOGY, Nov. 2006, p. 8099–8108 Vol. 26, No. 21
0270-7306/06/$08.00+0 doi:10.1128/MCB.01332-06

Hspa4l-Deficient Mice Display Increased Incidence of Male Infertility and Hydronephrosis Development[▽]

Torsten Held,[1] Ilona Paprotta,[1] Janchiv Khulan,[1] Bernhardt Hemmerlein,[2] Lutz Binder,[3] Stephan Wolf,[1] Stephanie Schubert,[4] Andreas Meinhardt,[5] Wolfgang Engel,[1] and Ibrahim M. Adham[1]*

Institute of Human Genetics,[1] Department of Pathology,[2] and Department of Clinical Chemistry,[3] University of Göttingen, Göttingen, Department of Human Genetics, Hannover Medical School, Hannover,[4] and Department of Anatomy and Cell Biology, University of Giessen, Giessen,[5] Germany

Received 20 July 2006/Accepted 15 August 2006

The *Hspa4l* gene, also known as *Apg1* or *Osp94*, belongs to the HSP110 heat shock gene family, which includes three genes encoding highly conserved proteins. This study shows that *Hspa4l* is expressed ubiquitously and predominantly in the testis. The protein is highly expressed in spermatogenic cells, from late pachytene spermatocytes to postmeiotic spermatids. In the kidney, the protein is restricted to cortical segments of distal tubules. To study the physiological role of this gene in vivo, we generated mice deficient in Hspa4l by gene targeting. Hspa4l-deficient mice were born at expected ratios and appeared healthy. However, approximately 42% of *Hspa4l*$^{-/-}$ male mice suffered from fertility defects. Whereas the seminiferous tubules of *Hspa4l*$^{-/-}$ testes contained all stages of germ cells, the number of mature sperm in the epididymis and sperm motility were drastically reduced. The reduction of the sperm count was due to the elimination of a significant number of developing germ cells via apoptosis. No defects in fertility were observed in female mutants. In addition, 12% of null mutant mice developed hydronephrosis. Concentrations of plasma and urine electrolytes in *Hspa4l*$^{-/-}$ mice were similar to wild-type values, suggesting that the renal function was not impaired. However, *Hspa4l*$^{-/-}$ animals were preferentially susceptible to osmotic stress. These results provide evidence that Hspa4l is required for normal spermatogenesis and suggest that Hspa4l plays a role in osmotolerance.

Cells respond to protein-denaturing stress, such as heat, by rapidly inducing the expression of a wide array of heat shock genes. Heat shock proteins (HSPs) are a group of highly conserved proteins that are expressed constitutively and/or induced by different kinds of stress. HSPs participate in protein folding and assembly, elimination of misfolded proteins, and stabilization of newly synthesized proteins in various intercellular compartments (9). These proteins have been divided into families based on their structural similarities and apparent molecular weights (4).

The HSP110/SSE gene family was shown to contain several distantly related genes, including two genes in *Saccharomyces cerevisiae* known as *SSE1* and *SSE2* (21, 25), the sea urchin sperm receptor gene (6), and several mammalian genes. The cellular functions of the HSP110/SSE gene family members are unclear. HSPs have been shown to prevent the aggregation of model substrates in vivo (7) and have been implicated in thermotolerance (23, 24). In *S. cerevisiae*, the loss of *SSE1* results in a reduction of cell proliferation and temperature sensitivity, whereas the loss of *SSE2* causes no overt phenotype (21). However, inactivation of both genes in some strain backgrounds is lethal (27).

The mammalian HSP110 gene family consists of the genes for three proteins, namely, Hspa4l (also known as Apg1 or Osp94), Hspa4 (also known as Apg2), and Hsp110. Constitutive expression of *Hspa4l* is high in the testis and moderate in other tissues, while *Hspa4* and *Hsp110* are ubiquitously expressed in various tissues (12, 13, 15, 20, 31).

Expression analyses of *Hspa4l* in the testes, inner medullary collection duct cell line (mIMCD3), and kidneys of a water-restricted mouse revealed an increase of *Hspa4l* expression by hyperosmotic NaCl or heat shock (12, 15). These results suggest that the *Hspa4l* gene is a hyperosmotic and heat stress-inducible member of the HSP110 family. The induction of *Hspa4l* gene expression is consistent with the observation that the 5′-flanking region of *Hspa4l* has functional tonicity (TonE)- and heat shock-responsive elements that respond independently to hypertonicity and heat stress, respectively (16).

With the exception of the sea urchin sperm receptor and yeast SSE proteins, the functions of the members of the HSP110/SSE family, including Hspa4l, are an enigma. Therefore, we determined the physiological function of Hspa4l in vivo by the generation of Hspa4l-deficient mice. Hspa4l deficiency did not impair development to adulthood but caused an increased incidence of male infertility characterized by reductions of sperm number and motility. In addition, approximately 12% of homozygous male mutants had unilateral hydronephrotic kidneys. An increased susceptibility of *Hspa4l*$^{-/-}$ mice to osmotic stress was observed. These various phenotypes, presumably due to differences in genetic background, provide evidence for multiple roles for Hspa4l in spermatogenesis and osmotic tolerance.

* Corresponding author. Mailing address: Institute of Human Genetics, Heinrich-Düker-Weg 12, D-37073 Göttingen, Germany. Phone: 49-551-397522. Fax: 49-551-399303. E-mail: iadham@gwdg.de.

▽ Published ahead of print on 21 August 2006.

MATERIALS AND METHODS

Generation of Hspa4l-deficient mice. Genomic 9.8- and 4.1-kb HindIII fragments containing the sequences of exons 1 and 2 of *Hspa4l*, respectively, were

isolated from a PAC clone (RPCIP711K23427Q2, RZPD) and cloned into the pZERO-TM-2 vector (Invitrogen). The numbering of these exons was based on a published exon/intron structure of the mouse *Hspa4l* gene (ENSMUSG25757). The *Hspa4l*-targeting vector was constructed using the plasmid vector pPNT (29). To generate the *Hspa4l*-targeting construct, the 6.5-kb EcoRI/SmaI fragment containing the sequence of the 5′-flanking region was used as a left arm (see Fig. 2A). This fragment was first cloned into pBluescript (Stratagene), excised as a BamHI/EcoRI fragment, and then cloned into the pPNT vector (clone Hspa4l-1). A 4.1-kb HindIII fragment containing exon 2 was used as the right arm and inserted in the HindIII restriction site of pBluescript, excised as a SalI/NotI fragment, and cloned into the XhoI/NotI sites of clone Hspa4l-1 (see Fig. 2A). The resulting Hspa4l-targeting vector was linearized with NotI and then transfected into RI embryonic stem (ES) cells (30), and colonies resistant to G418 (300 μg/ml) and ganciclovir (2 μM) were selected.

Genomic DNAs extracted from individual drug-resistant clones were screened for homologous recombination by Southern blot analysis. DNAs were digested with BamHI, separated in 0.8% agarose gels, and transferred to nylon membranes (Amersham Pharmacia, Braunschweig, Germany). A 0.5-kb fragment located 5′ of the targeting vector (see Fig. 2A) was amplified, radioactively labeled, and used to probe the Southern blots. Hybridization was carried out at 65°C overnight in a solution containing the following: 5× SSC (1× SSC is 0.15 M NaCl plus 0.015 M sodium citrate), 5× Denhardt's solution, 0.1% sodium dodecyl sulfate (SDS), and denatured salmon sperm DNA (100 μg/ml). Filters were washed twice at 65°C at a final stringency of 0.2× SSC–0.1% SDS. Cells from two recombinant ES cell clones were injected into C57BL/6J blastocysts, and these were transferred to DBA/BL6 pseudopregnant females. Germ line-transmitting chimeric males obtained from both lines were backcrossed to C57BL/6J and 129/Sv females, and the resulting F_1 offspring were genotyped by PCR analyses. Most studies were performed with homozygous mutants on a C57BL/6J × 129/Sv mixed genetic background and with their wild-type littermates. Mice were taken from the second or third generation produced by crossing a male chimera with a C57BL/6J female.

To genotype the mice, genomic DNAs were extracted from tails and analyzed by PCR. Thermal cycling was carried out for 35 cycles of denaturation at 94°C for 30 s, annealing at 55°C for 30 s, and extension at 72°C for 1 min. The following primers were used to discriminate between wild-type and mutant alleles. Primer Apg1-F1 (P1 sense [5′-GGTCAGAAAGGCTCACCAAGG-3′]) and primer Apg1-R2 (P2 antisense [5′-ACTGAGGCCCTTGATTTGGCC-3′]) were designed to amplify wild-type loci. The primer PGK1 (P3 antisense [5′-TCTGAG CCCAGAAAGCGAAGG-3′]) was designed to amplify the targeted locus (see Fig. 2A). A 213-bp fragment was amplified with primers P1 and P2 for the wild-type allele, whereas primers P2 and P3 amplified a 433-bp fragment of the mutant allele.

All animal experimentation was reviewed and approved by the Institutional Animal Care and Use Committee of the University of Göttingen.

Northern blots and reverse transcription-PCR (RT-PCR). Total RNA was extracted from tissues by using a QIAGEN RNA kit (QIAGEN, Hilden, Germany). For Northern blot analysis, 15 μg of RNA was electrophoresed in a 1.2% agarose gel containing 2.2 M formaldehyde, transferred to a nylon membrane, and hybridized with a ^{32}P-labeled probe under the same conditions as those used for Southern blot hybridization. A 206-bp fragment containing part of the 3′-untranslated region of the *Hspa4l* cDNA was amplified with the EST12-F1 primer (5′-CAGTTTGAGCTCTCCTTACATAC-3′) and the EST12-R1 primer (5′-CTGGTGGCTCTAAACCACATCGG-3′) and used as a probe for Northern blot hybridization.

RT-PCR assays were performed using 2 μg of total RNA and a One Step RT-PCR kit (QIAGEN). Primers to amplify the *Hspa4I* cDNA fragment containing the sequence of exons 1 to 4 were 5′-TCGGCTTCCTCAACTGCTAC-3′ and 5′-CTTCCAGGTACCGCACCTTA-3′, and those to amplify the *Hprt* transcript were 5′-CCTGCTGGATTACATTAAAGCACTG-3′ and 5′-GTCAAGG GCATATCCTACAACAAC-3′.

Fertility test. To investigate the fertility of the Hspa4l-deficient males on a hybrid 129/Sv × C57BL/6J and an inbred 129/Sv genetic background, sexually mature *Hspa4l*$^{-/-}$ males from the second generation were intercrossed, each with two wild-type CD1 females, for 3 months. Females were checked for the presence of vaginal plugs and/or pregnancy. Pregnant females were removed to holding cages to give birth. The number and size of litters sired by each group of males were determined for a 3-month mating period.

Sperm analysis. From *Hspa4l*$^{-/-}$ and *Hspa4l*$^{+/+}$ male mice of the hybrid genetic background, the epididymides were collected and dissected in Tyrode's medium. The sperm number in the cauda epididymis was determined using a Neubauer counting chamber. Motility was analyzed by a CEROS computer-assisted semen analysis system (version 10; Hamilton Thorne Research, Beverly, Mass.). Epididymides of *Hspa4l*$^{-/-}$ and *Hspa4l*$^{+/+}$ mice were dissected in in vitro fertilization medium (Medi-Cult, Jyllinge, Denmark). Sperm were allowed to swim out of the epididymides and incubated for 1.5 h at 37°C. Aliquots (5 μl) of sperm suspension were placed into a disposable counting chamber, which was set at a temperature of 37°C. Spermatozoa (6,000 to 10,000) from fertile and infertile *Hspa4l*$^{-/-}$ and *Hspa4l*$^{+/+}$ mice were analyzed using the following parameters: negative phase-contrast optics; recording at 60 frames/s; minimum contrast, 60; minimum cell size, 6 pixels; straightness (STR) threshold, ≥50%; cutoffs of average path velocity (VAP) and straight-line velocity (VSL), 25 and 30 μm/s, respectively; and minimum progressive VAP, 75 μm/s.

For statistical analysis, frequencies of the six sperm motility parameters, i.e., VAP, VSL, curved-line velocity (VCL), lateral head amplitude (ALH), beat cross frequency (BCF), and STR, were examined by probability plots categorized by mouse type (wild type or fertile or infertile *Hspa4l* mutant). VAP, VSL, VCL, and BCF were log normally distributed, but ALH and STR were not. Considering the log normal distribution, Student's *t* tests for independent observations were applied in order to define differences in VAP, VSL, VCL, and BCF means normalized by natural logarithms comparing wild-type mice and both groups of *Hspa4l*$^{-/-}$ mice. For the same purpose, the nonparametric ALH and STR distributions were tested by Friedman's analysis of variance. Statistical analyses were performed with Statistica (StatSoft, Inc., Tulsa, Okla.).

Histological analysis and TUNEL assay. Animals were killed by cervical dislocation. Testes and kidneys were isolated and fixed. From each male, one testis was fixed in Bouin's fixative for 24 h at room temperature, and the other testis was fixed in phosphate-buffered formalin for 24 h at 4°C. Subsequently, organs were embedded in paraffin. Mounted sections were deparaffinized, rehydrated, and stained with hematoxylin and eosin. For terminal deoxynucleotidyltransferase-mediated dUTP-biotin nick end labeling (TUNEL) analysis, formalin-fixed sections were deparaffinized, rehydrated, and pretreated with proteinase K (Roche Diagnostics). Apoptotic cells were detected using an ApopTag peroxidase in situ apoptosis detection kit (Qbiogene, Germany) according to the manufacturer's instructions. To determine the extent of apoptosis in testes, sections of testes derived from six 12-week-old *Hspa4l*$^{-/-}$ mice and from two age-related wild-type mice were subjected to TUNEL assay. The numbers of both TUNEL-positive and TUNEL-negative tubules were determined, and the number of TUNEL-positive cells per tubule was counted. The average for 10 to 20 fields for each testis was used, and the standard deviation (SD) was also determined for the examined fields.

Western blotting and immunohistochemistry. Tissues were lysed in RIPA buffer (Santa Cruz Biotechnology). Proteins were resolved by SDS-polyacrylamide gel electrophoresis and transferred to nitrocellulose membranes (Amersham Pharmacia). Blots were blocked with 5% skim milk in phosphate-buffered saline (PBS) before incubation with the primary antibodies in PBS with skim milk overnight at 4°C. After a washing step, bound antibodies were detected using horseradish peroxidase-conjugated anti-rabbit and anti-mouse immunoglobulin G (Sigma) and enhanced chemiluminescence (Pierce Chemical). The primary antibodies and dilutions used were rabbit anti-Hspa4l/Apg1 (N-96; Santa Cruz Biotechnology) at 1:500, rabbit anti-Hspa4/Apg2 (N-60; Santa Cruz Biotechnology) at 1:500, mouse anti-Hsp70 (C92; Stressgen) at 1:1,000, and mouse anti-Hsp90α (C-20; Santa Cruz Biotechnology) at 1:200.

For immunohistochemistry, formalin-fixed sections were preincubated for 1 h with 5% normal goat serum in 0.05% Triton X-100–PBS, incubated overnight at 4°C with 1:200 diluted rabbit anti-Hspa4l antibody, washed with PBS, and then incubated with alkaline phosphatase-conjugated goat anti-rabbit antibody at a 1:500 dilution (Sigma) for 1 h at room temperature. After a washing step with PBS, immunoreactivity was detected by incubating the sections with a solution containing Fast red TR/naphthol AS-MX phosphate tablets (Sigma).

Biochemical analysis of blood and urine. For the collection of urine samples, mice were kept in metabolic cages, and urine samples were collected over 24-h periods. Trunk blood was collected into heparinized tubes for analysis on an AVL OMNI9 (Roche, Mannheim, Germany) blood gas analyzer. Urine electrolytes were analyzed by flame photometry (Modular; Roche, Mannheim, Germany).

Electron microscopy. Testes and epididymides were fixed with 5% glutaraldehyde in 0.2 M phosphate buffer, postfixed with 2% osmium tetroxide, and embedded in epoxy (Epon) resin. Selected areas were then sectioned and examined by electron microscopy.

Statistical analysis. Paired comparisons of different sperm parameters and the apoptotic indexes in testes among *Hspa4l*$^{-/-}$ and *Hspa4l*$^{+/+}$ mice were performed to determine statistical significance by calculating means ± SD and using Student's *t* test.

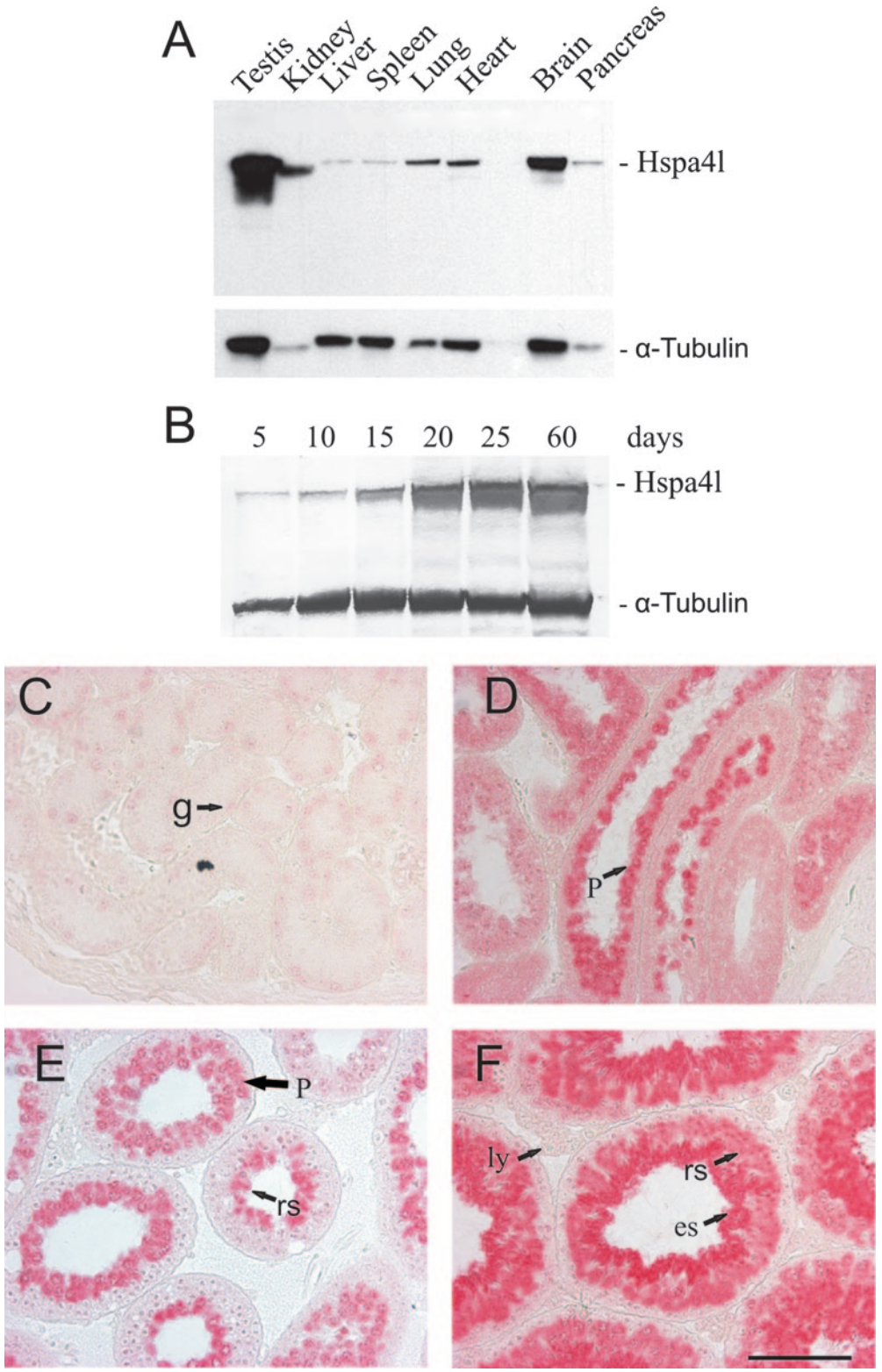

FIG. 1. Expression profile and cellular localization of Hspa4l during testis development. (A and B) Immunoblot analysis of Hspa4l in cellular extracts from different tissues (A) and from testes of 5-, 10-, 15-, 20-, 25-, and 60-day-old mice (B), using polyclonal antibodies against mouse Hspa4l. A monoclonal antibody against α-tubulin was used as a loading control. (C to F) Immunohistochemistry using the Hspa4l antibody on sections of 5 (C)-, 15 (D)-, 25 (E)-, and 60-day-old (F) testes. Weak expression of Hspa4l was seen in gonocytes (g) of the 5-day-old testis (C). Hspa4l was highly expressed in pachytene spermatocytes (p) of the 15-day-old testis (D). In testes of 25- and 60-day-old mice (E and F), the protein was highly accumulated in spermatogenic cells, from late pachytene spermatocytes to postmeiotic round (rs) and elongated (es) spermatids. Hspa4l-immunopositive staining was barely detectable in Leydig (ly) cells and spermatogonia (sg). Bar, 100 μm.

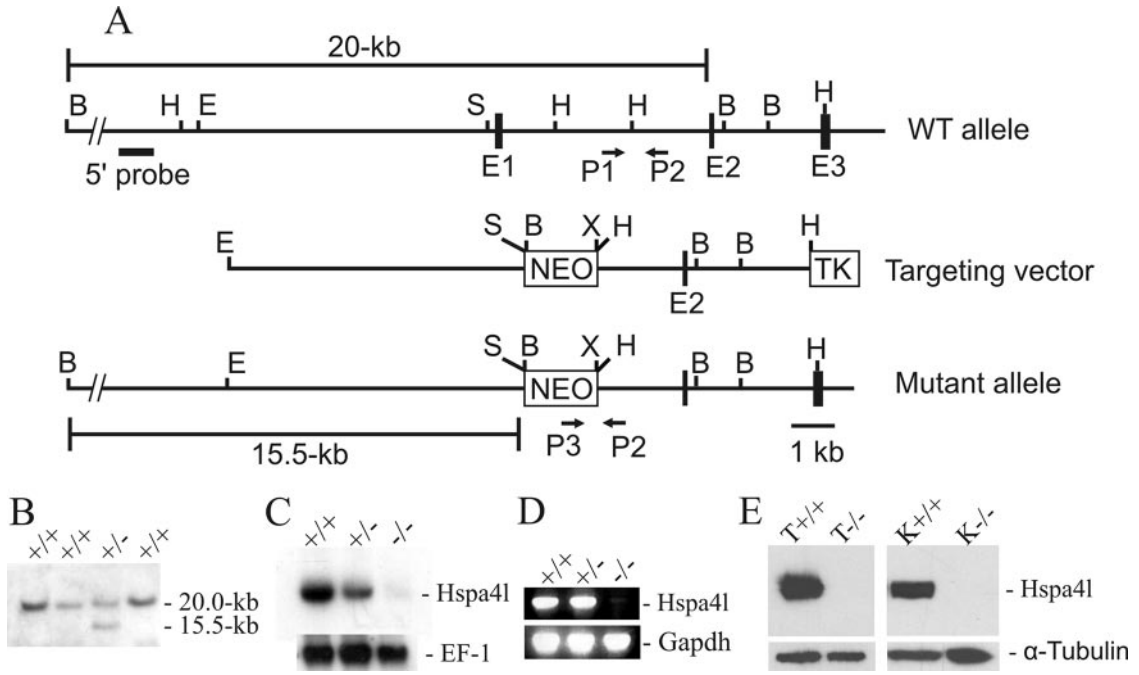

FIG. 2. Targeted disruption of *Hspa4l* gene. (A) Structures of the wild-type, targeted-vector, and recombinant alleles are shown together with the relevant restriction sites. The numbers under the rectangles indicate the exons of *Hspa4l*. A 2.5-kb SmaI/HindIII fragment containing exon 1 was replaced by a *pgk-neo* selection cassette (NEO). The 5′ external probe used and the predicted length of BamHI restriction fragments in Southern blot analysis are shown. The primers P1, P2, and P3 used to amplify the wild-type and mutant alleles by PCR are also indicated. Abbreviations: TK, thymidine kinase cassette; B, BamHI; E, EcoRI; H, HindIII; S, SmaI; X, XhoI. (B) Southern blot analysis of recombinant ES cell clones. Genomic DNAs extracted from ES cell clones were digested with BamHI and probed with the 5′ probe shown in panel A. The *Hspa4l* wild-type allele generated a 20.0-kb BamHI fragment, whereas the targeted allele yielded a 15.5-kb BamHI fragment, as indicated in panel A. (C) Northern blot analysis. Total RNAs of $Hspa4l^{-/-}$, $Hspa4l^{+/-}$, and $Hspa4l^{+/+}$ mice were hybridized with a cDNA probe containing the sequence of the 3′-untranslated region of *Hspa4l*. Rehybridization of blots with human elongation factor 1 cDNA (EF-1) revealed the integrity of RNA loading. (D) RT-PCR analysis using testicular RNA and primers located in exons 1 and 4 confirmed the absence of exon 1 in *Hspa4l* targeted transcripts. (E) Western blot with proteins extracted from testes (T) and kidneys (K) of $Hspa4l^{+/+}$ and $Hspa4l^{-/-}$ mice, probed with anti-Hspa4l antibodies. The immunoreactive 94-kDa Hspa4l protein was detectable in wild-type but not in $Hspa4l^{-/-}$ tissues.

RESULTS

Hspa4l mRNA expression in mouse testis. RNA analysis has shown that *Hspa4l* mRNA is expressed in all mouse tissues but is at the highest level in the testis (14). A similar expression pattern was also shown at the protein level (Fig. 1A). To evaluate the expression pattern of Hspa4l during testis development, we performed Western blot analysis using protein extracts from testes of 5-, 15-, 20-, 25-, and 60-day-old mice (Fig. 1B). The Hspa4l quantity was normalized against α-tubulin, and the relative quantity in each line was determined. This analysis revealed a low expression of Hspa4l in the testes of 5- and 10-day-old mice. By postnatal day 15, the level of Hspa4l increased and remained high thereafter (Fig. 1B). To ascertain whether a specific compartment of the testes shows high expression of the Hspa4l protein, immunohistochemistry was undertaken on testis sections from 5-, 15-, 25-, and 60-day-old mice (Fig. 1C to F). In testis sections from 5-day-old mice, Hspa4l-immunopositive staining was barely detectable in Sertoli and Leydig cells, while low levels of immunostaining for Hspa4l were seen in gonocytes (Fig. 1C). In testes of 15-day-old mice, the most intense immunoreactions were observed in pachytene spermatocytes (Fig. 1D). In testes of 25- and 60-day-old mice, Hspa4l protein was highly accumulated in spermatogenic cells, from late pachytene spermatocytes to round and elongating spermatids (Fig. 1E and F).

Targeted disruption of *Hspa4l*. To clarify the in vivo function of *Hspa4l*, the gene was disrupted by homologous recombination in ES cells, using a replacement targeting strategy (Fig. 2A). A Hspa4l-targeting construct was designed to replace a 2.5-kb SmaI/HindIII genomic fragment containing exon 1 with a neomycin resistance gene (neo^r) under the control of the *Pgk* promoter. Exon 1 contains the translation initiation codon ATG, and the expected targeting event would generate an allele that transcribes an untranslated *Hspa4l* mRNA.

Following electroporation and drug selection, homologous recombinants were detected by Southern blot analysis of BamHI-restricted genomic DNA, using a 5′ external probe (Fig. 2A). The external probe detected a 20.0-kb wild-type fragment and a 15.5-kb recombinant fragment (Fig. 2B). Two $Hspa4l^{+/-}$ ES cell clones injected into C57BL/6J blastocysts gave rise to chimeric mice that transmitted the *Hspa4l* mutation into the germ line. Chimeric mice were intercrossed with C57BL/6J or 129/Sv females to establish the *Hspa4l*-disrupted allele on a C57BL/6J × 129/Sv hybrid and on a 129/Sv inbred genetic background. The resulting progeny from the heterozygous intercrosses displayed a normal Mendelian ratio of

TABLE 1. Sperm analysis in *Hspa4l*$^{-/-}$ and *Hspa4*$^{+/+}$ mice[a]

Genotype and group	No. of sperm in cauda epididymis (10^6)	Sperm motility (%)	Progressive motility (%)
+/+	19.7 ± 0.8 (5)	61.7 ± 4.6 (6)	40.8 ± 5.1 (6)
−/−			
Group I	0.059 ± 0.03* (4)	8.5 ± 0.5* (4)	5.2 ± 0.3* (4)
Group II	16.9 ± 0.7 (6)	36.2 ± 6.2* (5)	19.6 ± 3.9* (5)

[a] Data for sperm analysis represent the means ± SD for the numbers of individual measurements indicated in parentheses. *, value in *Hspa4l*$^{-/-}$ mice is significantly different from that in *Hspa4*$^{+/+}$ mice ($P < 0.01$ by Student's *t* test). Groups I and II are infertile and fertile *Hspa4l*$^{-/-}$ males, respectively.

Hspa4l$^{+/+}$, *Hspa4l*$^{+/-}$, and *Hspa4l*$^{-/-}$ animals, indicating that Hspa4l is not essential for embryonic development. *Hspa4l*$^{-/-}$ mice were indistinguishable from their wild-type littermates in appearance and gross behavior.

To confirm that the engineered disruption of *Hspa4l* had generated a null mutation, we performed Northern blot and RT-PCR analyses on RNAs from testes of mice of the three genotypes. An *Hspa4l*-specific probe detected a weak band of reduced size in RNAs from *Hspa4l*$^{-/-}$ testes (Fig. 2C). RT-PCR with primers that encompass exons 1 and 4 was not able to amplify any *Hspa4l* cDNA from testicular RNAs from *Hspa4l*$^{-/-}$ mice (Fig. 2D). To confirm the inactivation of Hspa4l at the protein level, we performed Western blot analysis. An anti-Hspa4l antibody recognized the expected 94-kDa Hspa4l protein in the wild-type testis and kidney, while an Hspa4l protein of the same size was not discernible in either tissue from *Hspa4l*$^{-/-}$ mice (Fig. 2E).

Reproductive defects in *Hspa4l*$^{-/-}$ male mice. During attempts to establish a breeding colony from progeny of the F_2 generation, we found reduced offspring rates for cages of *Hspa4l*$^{-/-}$ mice on a C57BL/6J × 129/Sv mixed genetic background. Therefore, we investigated the fertility of *Hspa4l*$^{-/-}$ mice of both sexes with wild-type mates. Homozygous *Hspa4l*$^{-/-}$ females showed no severe reproductive defects and produced litters of approximately normal size (average litter size, 8.3 [$n = 15$]; average wild-type litter size, 9.6 [$n = 15$]). In contrast, the fertility of *Hspa4l*$^{-/-}$ males was reduced. Five *Hspa4l*$^{+/+}$ and 12 *Hspa4l*$^{-/-}$ males mated with wild-type females of strain CD1 over a period of 3 months produced averages of 14.4 and 5.7 offspring, respectively. Five of 12 *Hspa4l*$^{-/-}$ males (42%) produced no offspring but generated postcoital vaginal plugs in females, indicating that infertile males were capable of mating. The other seven *Hspa4l*$^{-/-}$ males produced small litter sizes (8.6 [$n = 21$]) compared to those of their wild-type littermates (14.4 [$n = 15$]). These results revealed that male fertility was heterogeneous and that homozygous mutant mice fell into two classes, as follows: group I males were infertile, whereas group II males were fertile. Similar observations were found for colonies with the 129/Sv inbred genetic background. We focused subsequent experiments on these two groups of animals.

To investigate the underlying cause of the reproductive defects in *Hspa4l*$^{-/-}$ males, sperm parameters were analyzed in great detail. As shown in Table 1, significant reductions in the mean number of spermatozoa and the proportions of motile and progressively motile sperm collected from the cauda epididymides of infertile *Hspa4l*$^{-/-}$ males were observed ($P < 0.001$), whereas fertile *Hspa4l*$^{-/-}$ males (group II) showed sperm at a normal concentration but with significantly reduced sperm motility compared with that for control littermates ($P < 0.01$). Computer-assisted sperm analysis showed that the mutant sperm's main motility parameters of VAP, VCL, and VSL were significantly impaired in both groups of Hspa4l-null mice (Fig. 3). Thus, Hspa4l deficiency results in a marked reduction of sperm motility.

Reduction of spermatogenesis and increased apoptosis of germ cells in *Hspa4l*$^{-/-}$ testes of infertile animals. To study the basis of reduced spermatogenesis in *Hspa4l*$^{-/-}$ males, histological sections of 3-month-old testes from infertile ($n = 3$) and fertile ($n = 3$) animals were examined. All stages of spermatogenesis could be recognized in the tubules of *Hspa4l*$^{-/-}$ testes (Fig. 4A and B). However, in sections of infertile mutants, the numbers of elongated spermatids were drastically reduced. Late spermatocytes, meiotic cells, and in particular haploid germ cells exhibited severe signs of degeneration ranging from nuclear condensation to cellular breakdown, vacuoles, premature release of germ cells into the lumen, and occasionally the presence of multinucleated giant cells (Fig. 4A and B). To determine if apoptosis contributed to the abnormality in the testes of *Hspa4l*$^{-/-}$ mice, a TUNEL assay was performed on testicular sections. For *Hspa4l*$^{-/-}$ mice, apoptotic cells were most commonly observed in adluminal regions of the seminiferous tubules (Fig. 4D). In contrast, apoptotic germ cells in wild-type testes were most frequently located close to the basement membranes of seminiferous tubules (Fig. 4C). The frequency of TUNEL-positive cells was variable among tubules, but overall there were significantly more apoptotic cells in the seminiferous tubules of infertile *Hspa4l*$^{-/-}$ mice than in those of their wild-type littermates (Fig. 4C and D). In contrast, TUNEL-positive cells were rarely found in the seminiferous tubules of fertile *Hspa4l*$^{-/-}$ mice (data not shown). Electron microscopy analysis confirmed the affected spermatogenesis in *Hspa4l*$^{+/+}$ testes in comparison to the wild type (Fig. 4E) and revealed that pachytene spermatocytes are the first cell population to be affected in *Hspa4l*$^{-/-}$ testes (Fig.

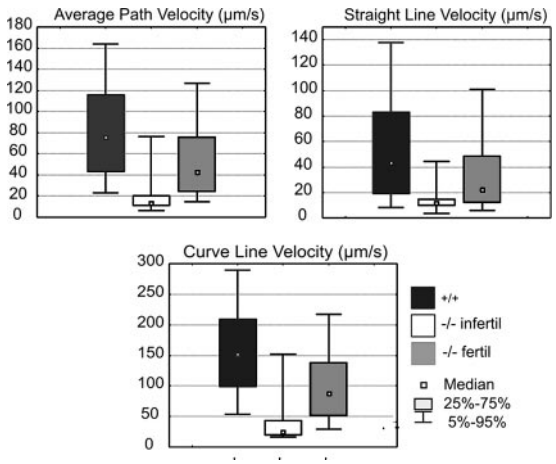

FIG. 3. Quantified sperm motility by computer-assisted sperm analysis. Sperm of fertile and infertile *Hspa4*$^{-/-}$ mice showed strongly reduced VCL, VAP, and VSL in comparison to spermatozoa of wild-type mice.

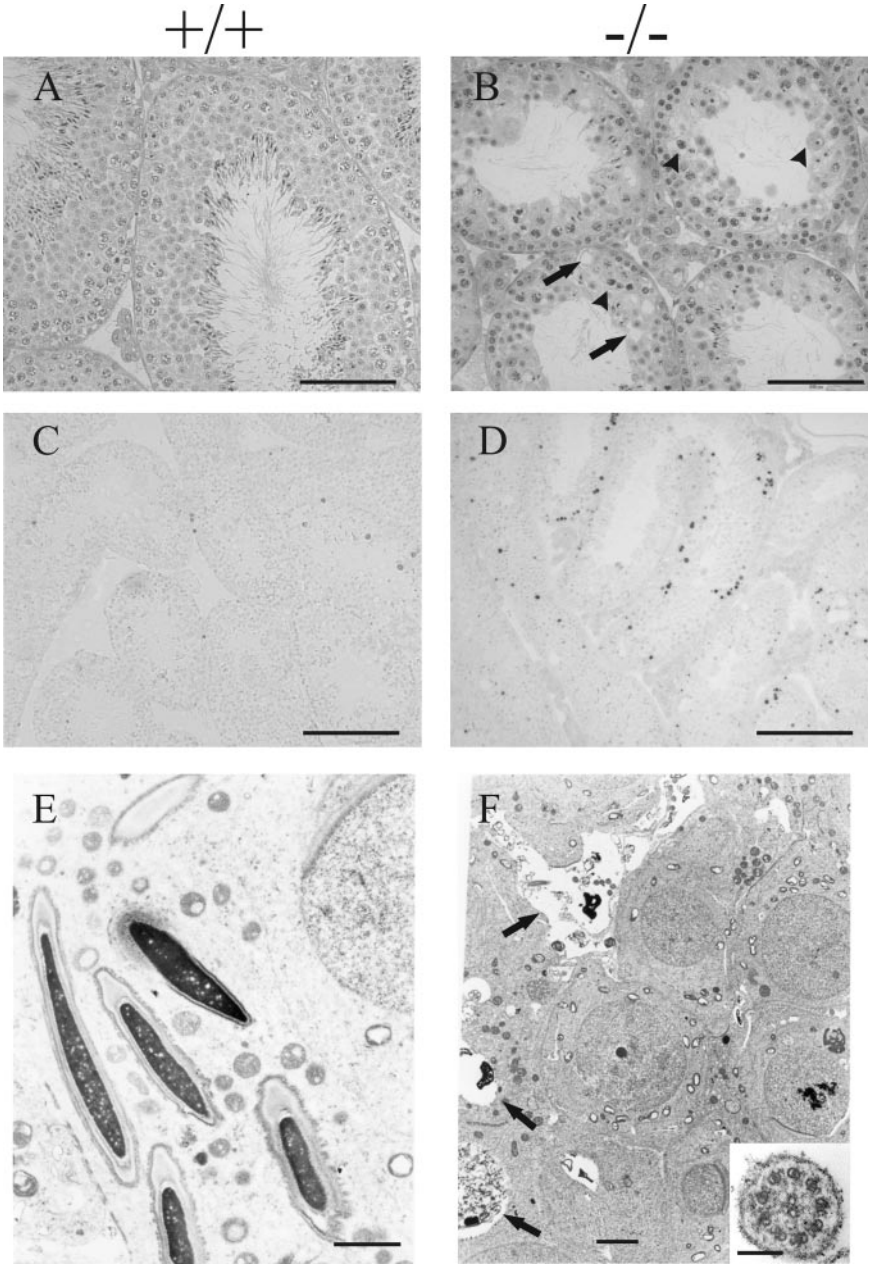

FIG. 4. Spermatogenesis in the testes of *Hspa4l*$^{-/-}$ mice. Histological sections from testes of 16-week-old wild-type (A, C, and E) and infertile *Hspa4l*$^{-/-}$ (B, D, and F) mice are shown. (A and B) Staining with hematoxylin and eosin revealed hypospermatogenesis with a strongly reduced number of elongated spermatids in the seminiferous tubules of *Hspa4*$^{-/-}$ mice (B) compared to those of their wild-type littermates (A). Degenerated spermatogenic cells (arrowheads), vacuoles (arrows), a decreased diameter of tubules, and the presence of multinucleated giant cells (not shown) were observed in testes of infertile *Hspa4l*$^{-/-}$ mice (B). In situ TUNEL staining in the seminiferous tubules of wild-type (C) and *Hspa4l*$^{-/-}$ (D) males revealed an increase in adluminal cells with darkly stained nuclei in a subset of the tubules in mutant testes (D), while apoptotic cells in wild-type testes were most frequently located close to the basement membranes of seminiferous tubules (C). Electron micrographs document normal spermatogenesis with round and elongating spermatids in *Hspa4l*$^{+/+}$ testes (E) and abnormal spermatogenesis in *Hspa4l*$^{-/-}$ testes (F). Arrows indicate several elongating spermatids at various stages of degeneration and vacuoles with cellular debris. Round spermatids reveal chromatin abnormalities and intracellular vacuoles, but these are much less prominent than in the later elongating spermatids. (Inset in panel F) Higher magnification of a cross section through a sperm flagellum showing the normal structure of the distal axoneme and microtubules. Bars: panels A and B, 200 μm; panels C and D, 100 μm; panel E, 2 μm; panel F, 1 μm; inset in panel F, 50 nm.

4F). No ultrastructural defects were detectable in the axonemal structures of epididymal sperm, suggesting that impaired sperm motility is not due to structural defects of the flagella (Fig. 4F).

Expression of HSPs in *Hspa4l*$^{-/-}$ testes. HSPs are a group of highly conserved proteins which are expressed constitutively and/or induced by stress. The expression of several HSP members is regulated during spermatogenesis. We examined the

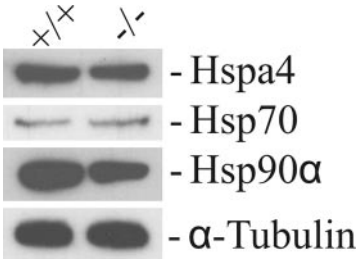

FIG. 5. Expression patterns of some HSPs in testes of wild-type and *Hspa4l*$^{-/-}$ mice. Proteins were isolated from testes of *Hspa4l*$^{+/+}$ and *Hspa4l*$^{-/-}$ mice and analyzed by Western blotting using the antibodies shown at the right.

expression of the homologous proteins Hspa4, Hsp70, and Hsp90α in *Hspa4l*$^{-/-}$ testes because overexpression of these proteins could theoretically compensate for the loss of Hspa4l expression. Testicular proteins derived from *Hspa4l*$^{+/+}$ and *Hspa4l*$^{-/-}$ animals were probed with anti-Hspa4, -Hsp70 and -Hsp90α antibodies. No marked change in the expression of these proteins was detected in the testes of Hspa4l-deficient mice (Fig. 5). These results suggest that the loss of Hspa4l expression in the testes is not compensated for by increased expression of Hspa4, Hsp70, and Hsp90α.

Hspa4l is constitutively expressed in the cortical distal segments of the nephron. Expression of the *Hspa4l* gene has been shown to be induced in the kidney in response to osmotic stress (15). To investigate the effect of osmotic stress on the expression profile of Hspa4l protein in the kidney and to determine the protein's cellular localization, we performed Western blot and immunohistochemical analyses. The levels of Hspa4l determined by immunoblotting were equivalent in kidneys of an untreated mouse, a water-restricted mouse, and a mouse treated with 3% NaCl in the drinking water (Fig. 6A). These results suggest that the expression of Hspa4l protein is not induced in response to osmotic stress. Immunohistological staining revealed that Hspa4l is restricted to epithelial cells of the cortical segments of the distal tubule (Fig. 6B). Immunoreactivity was absent from the glomerulus, the proximal tubule, and cells of the inner and outer medullas (Fig. 6B and data not shown). The Hspa4l-specific immunoreaction was confirmed by the absence of Hspa4l immunostaining in kidneys of Hspa4l-null mice (Fig. 6C).

Hydronephrosis development and loss of osmotolerance in Hspa4l-null mice. To determine the consequence of Hspa4l deficiency in the kidney, we analyzed the kidneys of *Hspa4l*$^{-/-}$ animals from the second and third generation. Of 66 Hspa4l-deficient mice at 4 to 8 months old, eight males (12%) exhibited massive unilateral or bilateral fluid-filled kidneys, whereas no abnormal phenotype was observed in kidneys of *Hspa4l*$^{+/+}$ and *Hspa4l*$^{+/-}$ littermates ($n = 94$). In all cases, the ureters were not enlarged or dilated, suggesting that a block in urine flow had occurred within the kidneys. All cases examined histologically showed moderate to severe dilation of the renal pelvis, a symptom that is indicative of hydronephrosis. In most cases, hydronephrosis was observed in the right kidney of male mice. The renal cortex was considerably thinned, and an enormously dilated renal pelvis surrounded the renal papilla in hydronephrotic kidneys. This was accompanied by different degrees of atrophy of the renal parenchyma (Fig. 6D and E). Unlike the case for the unaffected kidneys of other *Hspa4l*$^{-/-}$ animals, this difference was not found, although glomeruli and proximal and distal tubules from both hydronephrotic and unaffected kidneys of mutants were usually histologically indistinguishable from those of wild-type mice (Fig. 6F and G).

To address whether the loss of Hspa4l may impair renal function, we measured different parameters in blood and urine. Blood gases, pH, and serum and urinary electrolyte concentrations in *Hspa4l*$^{-/-}$ mice were within the physiological ranges and were similar to wild-type values (data not shown).

To determine the effects of osmotic stress on renal function, we exposed wild-type and mutant animals to osmotic stress by providing 3% NaCl in their drinking water for 14 days. In the first experiment, the body weights of three of six *Hspa4l*$^{-/-}$ mice were reduced 15 to 20% after 2 days of salt treatment, and the mice died on the third day. In contrast, all six wild-type animals overcame this procedure. We repeated the experiment on eight animals from both groups and evaluated their systemic electrolyte status and acid-base status in blood after 3 days of salt treatment. Three *Hspa4l*$^{-/-}$ mice were very weak on the third day of treatment. Blood parameters did not differ significantly between healthy animals in the two groups, but plasma Na^+, Ca^{2+}, and blood gases and urea nitrogen were significantly elevated in the three weakened *Hspa4l*$^{-/-}$ mice (Table 2).

DISCUSSION

The expression profile for the Hspa4l protein confirms and extends earlier Northern blotting results showing the high level of Hspa4l in the testis. Hspa4l expression was widespread but not ubiquitous. There was a specific pattern of expression in differentiated cell types, such as testis and kidney cells. Immunohistochemistry showed the high accumulation of Hspa4l in spermatogenic cells, from late pachytene spermatocytes to spermatids. In the kidney, Hspa4l was restricted to epithelial cells of the cortical distal tubules. The preferential expression of Hspa4l prompted us to investigate the specific role of Hspa4l in fertility and renal function by the generation of Hspa4l-deficient mice. Hspa4l-null mice were viable and did not exhibit obvious abnormalities, although Hspa4l expression has been detected in all tissues. Male infertility was the most apparent phenotype for *Hspa4l*$^{-/-}$ mice. Breeding of Hspa4l-null males with wild-type females revealed that the average litter size per male varied considerably, ranging from no pups born (infertile male group) to a smaller litter size than normal. This study has shown that the absence of Hspa4l does not significantly affect female reproduction.

Infertility in Hspa4l-deficient males cannot be ascribed to a disruption of spermatogenesis. All stages of spermatogenic cells were found in the Hspa4l-deficient testis. The increased number of apoptotic spermatocytes in testes of infertile *Hspa4l*$^{-/-}$ mice may be the cause of reduction in sperm number in the epididymis. Determination of sperm motility revealed that the progressive movement was abolished in a significant number of spermatozoa from both fertile and subfertile *Hspa4l*$^{-/-}$ mice. The striking feature of reduced sperm motility can be due either to a possible structural defect or to a functional blockade in a physiological process leading to

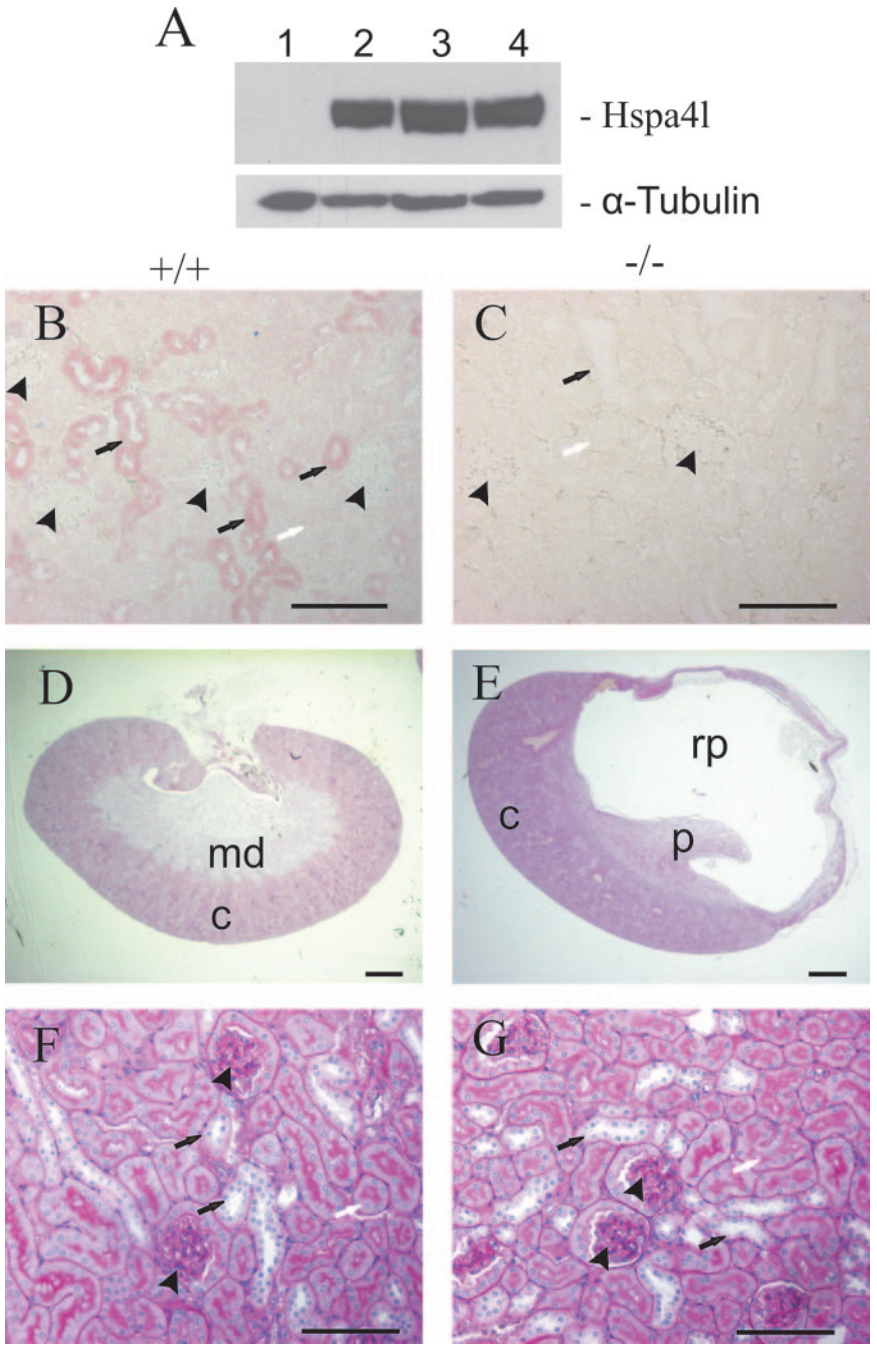

FIG. 6. Expression of Hspa4l in kidneys and histological analysis of hydronephrosis in Hspa4l-deficient mice. (A) Immunoblot with proteins extracted from kidneys of a Hspa4l-null mouse (lane 1), an untreated mouse (lane 2), a water-deprived mouse (lane 3), and a mouse treated with 3% NaCl in the drinking water (lane 4). The blot was incubated with anti-Hspa4l and -α-tubulin antibodies. (B and C) Immunohistological staining of renal sections from wild-type and Hspa4l-null mice with anti-Hspa4l antibody. Views at the level of the cortex show the localization of Hspa4l in the cytoplasm of epithelial cells of distal tubules (B). In contrast, there was no immunostaining in kidneys of null mice (C). (D and E) Whole kidney images of renal sections from wild-type (D) and Hspa4l-deficient (E) mice at 5 months old. The renal pelvis was grossly dilated in mutant mice. Detailed images of sections from a wild-type kidney (F) and a hydronephrotic kidney (G) at the level of the cortex do not show detectable structural changes in glomeruli (arrowheads) or proximal (white arrows) and distal (black arrows) tubules. c, cortex; md, medulla; p, papilla; rp, renal pelvis. Bars: panels D and E, 1 mm; panels B, C, F, and G, 200 μm.

the promotion of sperm motility. The normal development of Hspa4l-deficient sperm and the normal appearance of the axonemal ultrastructure, as shown by electron microscopy analysis, exclude a role for Hspa4l in the structural function of flagella. Therefore, the mobility defect can be attributed to the involvement of Hspa4l, directly or indirectly, in the biochemical pathway leading to acquisition of sperm motility. Recently, it was shown that Hspa4l, Hspa4, and Hsp70 are major cal-

TABLE 2. Blood data for 8-week-old *Hspa4l*$^{-/-}$ and *Hspa4*$^{+/+}$ mice treated with 3% NaCl in drinking water[a]

Genotype and group (*n*)	pH	pCO_2 (mm Hg)	pO_2 (mm Hg)	Concn in plasma (mmol/liter)			Hematocrit (%)	Blood urea nitrogen (mg/dl)
				Na^+	Ca^{2+}	K^+		
+/+ (7)	7.29 ± 0.04	60.79 ± 5.73	40.73 ± 3.97	160.02 ± 7.92	1.3 ± 0.04	7.18 ± 0.59	45.43 ± 3.99	28.25 ± 4.82
−/−								
Group I (3)	7.08 ± 0.09**	81.40 ± 16.19*	67.03 ± 5.09**	198.70 ± 16.21**	1.67 ± 0.09**	5.97 ± 1.47	41.63 ± 3.38	62.50 ± 1.41**
Group II (5)	7.32 ± 0.05	53.87 ± 5.1	34.55 ± 6.2	157.57 ± 3.64	1.32 ± 0.03	7.55 ± 0.51	43.15 ± 0.64	17.40 ± 1.47*

[a] All values are means ± SD. Asterisks indicate that values for *Hspa4l*$^{-/-}$ mice are significantly different from those for *Hspa4l*$^{+/+}$ mice (*, $P < 0.01$; **, $P < 0.001$ [Student's *t* test]). Groups I and II are susceptible and nonsusceptible *Hspa4l*$^{-/-}$ animals, respectively, with regard to treatment with 3% NaCl in their drinking water.

modulin (CaM) binding proteins in spermatogenic cells (19). CaMs regulate the activity of enzymes such as adenylate cyclases (8, 18) and protein kinases (10), which are involved in the regulation of flagellum bending (5, 28). The association of Hspa4l with other chaperons which assist in protein folding suggests a role for Hspa4l in the stabilization of signaling proteins controlling sperm motility.

Hspa4l-null mice were born at expected Mendelian ratios and displayed no overt disease phenotype. Subsequent analyses revealed the development of uni- and bilateral hydronephrosis in a small proportion of *Hspa4l*$^{-/-}$ mice, predominantly in male null mice. Hydronephrosis occurs due to an obstruction of urinary flow distal to the renal pelvis (i.e., at the level of the bladder or urethra) or, occasionally, in association with reflux nephropathy (2). The facts that unilateral hydronephrosis was frequently observed in Hspa4l-null mice and that the bladder and distal urethra were normal while the pelvis was dilated point to a pelviureteric junction as the site of obstruction. Congenital hydronephrosis in humans and several gene-deficient mouse lines, such as Agtr2- and Id2-null mice, appears predominantly in males, in a highly asymmetrical manner (1, 3, 11, 22). The mode of inheritance is not typical Mendelian, but instead, there is incomplete penetrance (17). For example, hydronephrosis is inherited with 21% penetrance in an inbred line of Agtr2-deficient males. However, the incidence of hydronephrosis in Agtr2-deficient mice was relatively lower in other inbred genetic backgrounds (22). Normal mice rarely develop hydronephrosis, with a reported incidence of 0.5 to 1.5% for a certain C57BL strain (26). However, hydronephrosis is shown in *Hspa4l*$^{-/-}$ mice with a hybrid C57BL/6J × 129/Sv genetic background but not in those with the inbred 129/Sv genetic background (data not shown). Furthermore, a high incidence of hydronephrosis was observed for the F_2 generation, which contains a high level of genetic variability between offspring. The decreased incidence of hydronephrosis in subsequent generations would impose a selection bias against that genotype. The variable incidence of hydronephrosis in both Hspa4l mutant lines may reflect the segregation of genetic modifiers on the mixed genetic background. Testing this possibility must await the backcrossing of Hspa4l-deficient mice onto a congenic C57BL/6J background.

Up-regulation of the *Hspa4l* gene in kidney and renal cell lines by osmotic stress suggested that Hspa4l may function to enable the kidney to compensate for osmotic stress present within the kidney (15). However, Western blot analysis did not display markedly elevated Hspa4l protein in kidneys of mice subjected to hyperosmolality. Immunohistochemistry localized Hspa4l to cortical segments of the distal nephron, which reabsorbs 20 to 30% of the NaCl from filtered urine. The NaCl reabsorption in distal tubules is accomplished with water reabsorption in subsequent collecting ducts. Water reabsorption from filtered urine is essential to avoid dehydration. Despite its specific localization in the kidney, Hspa4l deficiency does not have deleterious effects on renal function under physiological conditions. However, Hspa4l deficiency in mice maintained under conditions of hyperosmolality may result in decreased NaCl reabsorption in distal tubules, which will reduce the medullary interstitial osmolality and, as a result, decrease the driving force for water retention in outer medullary collecting ducts. Increased water loss may be responsible for the marked dehydration and significant increases in serum Na^+, Ca^{2+}, and urea nitrogen concentrations which were observed in some *Hspa4l*$^{-/-}$ mice treated with 3% NaCl in their drinking water. These results suggest that Hspa4l plays a critical role in enabling epithelial cells to adapt to high physiological osmotic stress.

The murine genome comprises three members of the Hsp110 family. The Hspa4 protein shows about 65% sequence identity with Hspa4l and is also expressed in a wide variety of tissues in the mouse (13). The viable phenotypes among Hspa4l-null mice led us to consider the possibility that the loss of Hspa4l function is compensated for by the expression of Hspa4. We tested this hypothesis by examining Hspa4 expression in the testes and kidneys of *Hspa4l*$^{-/-}$ mice. No evidence for up-regulation of Hspa4 was found. To definitively rule out the possibility that Hspa4 expression is able to compensate for the loss of Hspa4l in Hspa4l$^{-/-}$ mice, it will be necessary to generate mice that are null for both Hspa4l and Hspa4.

ACKNOWLEDGMENTS

We thank M. Schindler and H. Riedesel for their help in the generation and breeding of knockout mice. We also thank C. Müller for his help with particular experiments and R. M. Sharpe (MRC, Edinburgh, Scotland) for critically reading the manuscript.

This study was supported by grant AD129/2-2 from Deutsche Forschungsgemeinschaft.

REFERENCES

1. **Aoki, Y., S. Mori, K. Kitajima, O. Yokoyama, H. Kanamaru, K. Okada, and Y. Yokota.** 2004. Id2 haploinsufficiency in mice leads to congenital hydronephrosis resembling that in humans. Genes Cells **9:**1287–1296.
2. **Brown, T., J. Mandell, and R. L. Lebowitz.** 1987. Neonatal hydronephrosis in the era of sonography. Am. J. Roentgenol. **148:**959–963.
3. **Coret, A., B. Morag, M. Katz, D. Lotan, Z. Heyman, and M. Hertz.** 1994. The impact of fetal screening on indications for cystourethrography in infants. Pediatr. Radiol. **24:**516–518.
4. **Craig, E. A., J. S. Weissman, and A. L. Horwich.** 1994. Heat shock proteins and molecular chaperones: mediators of protein conformation and turnover in the cell. Cell **78:**365–372.
5. **Esposito, G., B. S. Jaiswal, F. Xie, M. A. Krajnc-Franken, T. J. Robben,**

A. M. Strik, C. Kuil, R. L. Philipsen, M. van Duin, M. Conti, and J. A. Gossen. 2004. Mice deficient for soluble adenylyl cyclase are infertile because of a severe sperm-motility defect. Proc. Natl. Acad. Sci. USA **101:** 2993–2998.

6. **Foltz, K. R., J. S. Partin, and W. J. Lennarz.** 1993. Sea urchin egg receptor for sperm: sequence similarity of binding domain and hsp70. Science **259:** 1421–1425.
7. **Goeckeler, J. L., A. Stephens, P. Lee, A. J. Caplan, and J. L. Brodsky.** 2002. Overexpression of yeast Hsp110 homolog Sse1p suppresses ydj1-151 thermosensitivity and restores Hsp90-dependent activity. Mol. Biol. Cell **13:**2760–2770.
8. **Gross, M. K., D. G. Toscano, and W. A. Toscano.** 1987. Calmodulin-mediated adenylate cyclase from mammalian sperm. J. Biol. Chem. **262:**8672–8676.
9. **Hartl, F. U., and M. Hayer-Hartl.** 2002. Molecular chaperones in the cytosol: from nascent chain to folded protein. Science **295:**1852–1858.
10. **Hook, S. S., and A. R. Means.** 2001. Ca^{2+}/CaM-dependent kinases: from activation to function. Annu. Rev. Pharmacol. Toxicol. **41:**471–505.
11. **Johnston, J. H., J. P. Evans, K. I. Glassberg, and S. R. Shapiro.** 1977. Pelvic hydronephrosis in children: a review of 219 personal cases. J. Urol. **117:**97–101.
12. **Kaneko, Y., H. Nishiyama, K. Nonoguchi, H. Higashitsuji, M. Kishishita, and J. Fujita.** 1997. A novel hsp110-related gene, apg-1, that is abundantly expressed in the testis responds to a low temperature heat shock rather than the traditional elevated temperatures. J. Biol. Chem. **272:**2640–2645.
13. **Kaneko, Y., T. Kimura, M. Kishishita, Y. Noda, and J. Fujita.** 1997. Cloning of apg-2 encoding a novel member of heat shock protein 110 family. Gene **189:**19–24.
14. **Kaneko, Y., T. Kimura, H. Nishiyama, Y. Noda, and J. Fujita.** 1997. Developmentally regulated expression of APG-1, a member of heat shock protein 110 family in murine male germ cells. Biochem. Biophys. Res. Commun. **233:**113–116.
15. **Kojima, R., J. Randall, B. M. Brenner, and S. R. Gullans.** 1996. Osmotic stress protein 94 (Osp94). A new member of the Hsp110/SSE gene subfamily. J. Biol. Chem. **271:**12327–12332.
16. **Kojima, R., J. D. Randall, E. Ito, H. Manshio, Y. Suzuki, and S. R. Gullans.** 2004. Regulation of expression of the stress response gene, Osp94: identification of the tonicity response element and intracellular signalling pathways. Biochem. J. **380:**783–794.
17. **Larson, R. S., M. A. Rudloff, H. Liapis, J. L. Manes, R. Davila, and J. Kissane.** 1995. The Ivemark syndrome: prenatal diagnosis of an uncommon cystic renal lesion with heterogeneous associations. Pediatr. Nephrol. **9:**594–598.
18. **Mons, N., J. L. Guillou, and R. Jaffard.** 1999. The role of Ca^{2+}/calmodulin-stimulable adenylyl cyclases as molecular coincidence detectors in memory formation. Cell. Mol. Life Sci. **55:**525–533.
19. **Moriya, M., M. Ochiai, H. J. Yuasa, N. Suzuki, and M. Yazawa.** 2004. Identification of Ca^{2+}-dependent calmodulin-binding proteins in rat spermatogenic cells as complexes of the heat-shock proteins. Mol. Reprod. Dev. **69:**316–324.
20. **Morozov, A., J. Subjeck, and P. Raychaudhuri.** 1995. HPV16 E7 oncoprotein induces expression of a 110 kDa heat shock protein. FEBS Lett. **371:**214–218.
21. **Mukai, H., T. Kuno, H. Tanaka, D. Hirata, T. Miyakawa, and C. Tanaka.** 1993. Isolation and characterization of SSE1 and SSE2, new members of the yeast HSP70 multigene family. Gene **132:**57–66.
22. **Nishimura, H., E. Yerkes, K. Hohenfellner, Y. Miyazaki, J. Ma, T. E. Hunley, H. Yoshida, T. Ichiki, D. Threadgill, J. A. Phillips III, B. M. Hogan, A. Fogo, J. W. Brock III, T. Inagami, and I. Ichikawa.** 1999. Role of the angiotensin type 2 receptor gene in congenital anomalies of the kidney and urinary tract, CAKUT, of mice and men. Mol. Cell **3:**1–10.
23. **Oh, H. J., X. Chen, and J. R. Subjeck.** 1997. Hsp110 protects heat-denatured proteins and confers cellular thermoresistance. J. Biol. Chem. **272:**31636–31640.
24. **Santos, B. C., A. Chevaile, R. Kojima, and S. R. Gullans.** 1998. Characterization of the Hsp110/SSE gene family response to hyperosmolality and other stresses. Am. J. Physiol. **274:**F1054–F1061.
25. **Shirayama, M., K. Kawakami, Y. Matsui, K. Tanaka, and A. Toh-e.** 1993. MSI3, a multicopy suppressor of mutants hyperactivated in the RAS-cAMP pathway, encodes a novel HSP70 protein of Saccharomyces cerevisiae. Mol. Gen. Genet. **240:**323–332.
26. **Taylor, D. M., and H. Fraser.** 1973. Hydronephrosis in inbred strains of mice with particular reference to the BRVR strain. Lab. Anim. **7:**229–236.
27. **Trott, A., L. Shaner, and K. A. Morano.** 2005. The molecular chaperone Sse1 and the growth control protein kinase Sch9 collaborate to regulate protein kinase A activity in Saccharomyces cerevisiae. Genetics **170:**1009–1021.
28. **Turner, R. M.** 2003. Tales from the tail: what do we really know about sperm motility? J. Androl. **24:**790–803.
29. **Tybulewicz, V. L., C. E. Crawford, P. K. Jackson, R. T. Bronson, and R. C. Mulligan.** 1991. Neonatal lethality and lymphopenia in mice with a homozygous disruption of the c-abl proto-oncogene. Cell **65:**1153–1163.
30. **Wurst, W., and A. L. Joyner.** 1993. Production of targeted embryonic stem cell clones, p. 33–61. *In* A. L. Joyner (ed.), Gene targeting: a practical approach. IRL Press, Oxford, England.
31. **Yasuda, K., A. Nakai, T. Hatayama, and K. Nagata.** 1995. Cloning and expression of murine high molecular mass heat shock proteins, HSP105. J. Biol. Chem. **270:**29718–29723.